*Radio Science*, Volume 27, Number 5, Pages 611–622, September–October 1992

# Transient scattering from dielectric cylinders: E-field, H-field, and combined field solutions

Douglas A. Vechinski and Sadasiva M. Rao

Department of Electrical Engineering, Auburn University, Auburn, Alabama

(Received September 26, 1991; revised March 10, 1992; accepted April 7, 1992.)

In this work, the problem of transient scattering by arbitrarily shaped two-dimensional dielectric cylinders is solved using the marching-on-in-time technique. The dielectric problem is approached via the equivalence principle. Three different formulations, namely, the electric field integral equation formulation, the magnetic field integral equation formulation, and the combined field integral equation formulation are considered. Numerical results are presented for two cross sections, namely, a circle and a square, and compared with inverse discrete Fourier transform (IDFT) techniques. In each case, good agreement is obtained with the IDFT solution.

## 1. INTRODUCTION

In recent times, the numerical solution of scattering problems directly in the time domain has received considerable attention mainly owing to the availability of fast computers. Of all the available time domain techniques, only the marching-on-in-time technique, developed by *Bennett* [1968], deals with the solution of integral equations, wherein the domain of the problem is confined to the scattering structure. Several cases have been studied using this technique involving one-dimensional [*Miller et al.*, 1973], two-dimensional [*Damaskos et al.*, 1985], and three-dimensional [*Bennett and Ross*, 1978; *Rao and Wilton*, 1991] structures. Please note that no attempt is made to cite all the references. However, one common problem associated with the marching-on-in-time technique is the occurrence of late-time oscillations. Various different reasons were attributed for these instabilities such as insufficient sampling, accumulation of round-off/truncation errors and so on. Of late, a series of papers were published by *Smith* [1990], *Rynne and Smith* [1990], and *Rynne* [1991] suggesting that these instabilities are mainly due to the nonuniqueness of the solution of the integral equation at certain characteristic frequencies. Our objective in this work is to verify this claim by developing alternate formulations which are free from the nonuniqueness problem and examining them.

It is well known that the dielectric cylinder problem can be formulated in three different ways using the equivalence principle, namely, the electric field integral equation (EFIE) formulation, the magnetic field integral equation (HFIE) formulation, and the combined field integral equation (CFIE) formulation [*Kishk and Shafai*, 1986]. It is also known, from the experience in frequency domain solutions, that both the EFIE and HFIE exhibit nonuniqueness at certain frequencies of the incident wave whereas the CFIE generates a unique solution at all frequencies [*Mautz and Harrington*, 1978]. However, as presented in the following, when attempted in the time domain, all the three formulations exhibit late-time oscillations suggesting that these oscillations are not entirely due to the internal resonances alone.



Paper number 92RS00964.
0048-6604/92/92RS-00964$08.00

## 2. INTEGRAL EQUATION FORMULATION

Consider an arbitrary shaped dielectric cylinder infinite in length along the $z$ axis. Let the cross section be denoted by some contour $C$. At each point on $C$ let $\hat{\mathbf{a}}_n$ represent an outward-directed unit vector normal to the contour. The circumferential vector, $\hat{\mathbf{a}}_\xi$, is then obtained by $\hat{\mathbf{a}}_\xi = \hat{\mathbf{a}}_z \times \hat{\mathbf{a}}_n$. The cylinder has material parameters of $\mu_d$ and $\varepsilon_d$, while exterior to the cylinder is a homogeneous medium with parameters $\mu_e$ and $\varepsilon_e$. The total fields exterior to the cylinder are designated by $\mathcal{E}_e$ and $\mathcal{H}_e$, while interior to the cylinder the fields are given by $\mathcal{E}_d$ and $\mathcal{H}_d$. The incident field is a plane wave with its electric field polarized in the $z$ direction (transverse magnetic (TM) incidence). The transverse electric (TE) solution may be obtained through the use of duality.

The equivalence principle will be employed to split the original problem into two separate problems. One is where the fields are equivalent external to the body, and the other is where the fields are equivalent internal to the body. The original problem is shown in Figure 1a and the equivalent exterior problem in Figure 1b. In this case, we restrict that only the fields exterior to the body remain the same. Then, we are free to choose what the interior fields are to be. For simplicity, the interior fields will be set to zero, and

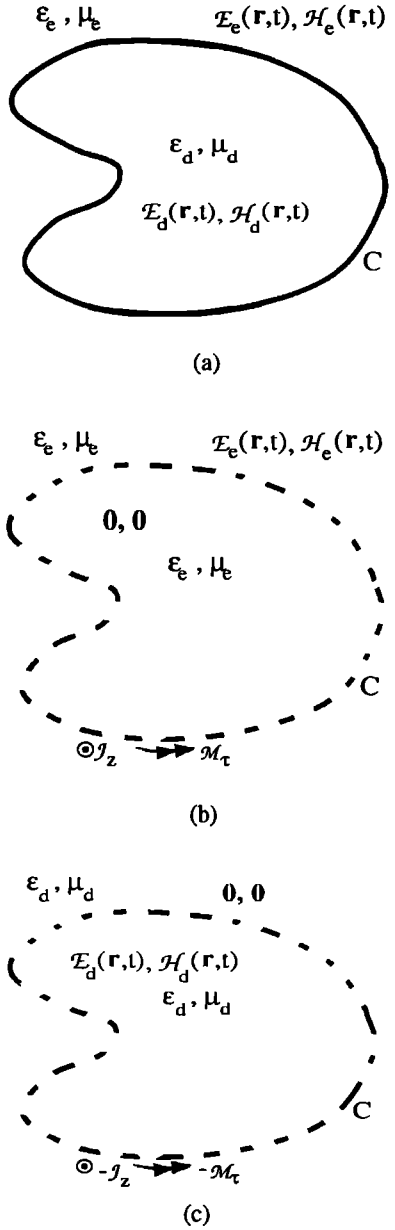


Fig. 1. Application of the equivalence principle. (a) Original problem, (b) exterior equivalent problem, and (c) Interior equivalent problem.

the interior material parameters will be set to be the same as those external to the body. Since the tangential fields are no longer continuous (i.e., some finite value outside and zero inside), equivalent electric currents, $\mathcal{J}$, and magnetic currents, $\mathcal{M}$, are required along the contour $C$ to make up for this discontinuity. For TM incidence, the electric currents are only in the $\hat{\mathbf{a}}_z$, direction while the magnetic currents are in the $\hat{\mathbf{a}}_\xi$ direction. These currents are now radiating in a homogeneous unbounded medium so that we may use the free space Green's function for the vector and scalar potentials. If we take any point inside $C$, we require that the sum of the incident field and the scattered field (due to the currents) combine to zero. Let $C^-$ designate points just inside the contour $C$, then

$$[\mathcal{E}_e^s[\mathcal{J},\mathcal{M}]+\mathcal{E}^{\text{inc}}]_{\tan} = 0 \quad \text{on } C^-, \quad (1)$$

$$[\mathcal{H}_e^s[\mathcal{J},\mathcal{M}]+\mathcal{H}^{\text{inc}}]_{\tan} = 0 \quad \text{on } C^-. \quad (2)$$

Similarly, we can form an equivalent interior problem (see Figure 1c), where the external fields have been set to zero and the exterior material parameters are set to the interior parameters. As before, equivalent currents along $C$ are set up to satisfy the discontinuity in the fields. It turns out that these equivalent currents are just the negative of the currents for the exterior equivalent problem. Here we require that the fields radiated by these currents are zero for any point exterior to the body. Specifically, for points just outside $C$ ($C^+$), we have

$$[\mathcal{E}_d^s[-\mathcal{J},-\mathcal{M}]]_{\tan}=0 \Longrightarrow [\mathcal{E}_d^s[\mathcal{J},\mathcal{M}]]_{\tan}=0 \text{ on } C^+ (3)$$

$$[\mathcal{H}_d^s[-\mathcal{J},-\mathcal{M}]]_{\tan}=0 \Longrightarrow [\mathcal{H}_d^s[\mathcal{J},\mathcal{M}]]_{\tan}=0 \text{ on } C^+ (4)$$

We now have four equations with which to solve for the two unknowns $\mathcal{J}$ and $\mathcal{M}$. The EFIE formulation is obtained by using equations (1) and (3) since only the electric field is involved. Similarly, the HFIE is formed by using equations (2) and (4). The CFIE may be obtained by using $[\alpha(1) + \hat{\mathbf{a}}_n \times \eta_e(1-\alpha)(2)]$ and $[\alpha(3) + \hat{\mathbf{a}}_n \times \eta_e(1-\alpha)(4)]$, where $0 \le \alpha \le 1$ and $\eta_e$ is the wave impedance in the external medium.

The scattered fields radiated by the equivalent electric and magnetic currents may be written in terms of the electric and magnetic vector and scalar potentials. That is,

$$\mathcal{E}_\nu^s[\mathcal{J},\mathcal{M}] = -\frac{\partial \mathcal{A}_\nu}{\partial t} - \frac{1}{\varepsilon_\nu}\nabla \times \mathcal{F}_\nu, \quad (5)$$

$$\mathcal{H}_\nu^s[\mathcal{J},\mathcal{M}] = -\frac{\partial \mathcal{F}_\nu}{\partial t} - \nabla\Phi_\nu^m + \frac{1}{\mu_\nu}\nabla \times \mathcal{A}_\nu, \quad (6)$$

where

$$\mathcal{A}_\nu(\mathbf{r},t) = \frac{\mu_\nu}{4\pi}\int_C\int_{z'=-\infty}^{\infty} \frac{\mathcal{J}(\mathbf{r}',t-\frac{R}{c_\nu})}{R}\,dz'\,dC', \quad (7)$$

$$\mathcal{F}_\nu(\mathbf{r},t) = \frac{\varepsilon_\nu}{4\pi}\int_C\int_{z'=-\infty}^{\infty} \frac{\mathcal{M}(\mathbf{r}',t-\frac{R}{c_\nu})}{R}\,dz'\,dC', \quad (8)$$

$$\Phi_\nu^m(\mathbf{r},t) = \frac{1}{4\pi\mu_\nu}\int_C\int_{z'=-\infty}^{\infty} \frac{\rho_s^m(\mathbf{r}',t-\frac{R}{c_\nu})}{R}\,dz'\,dC' \quad (9)$$

$R = |\mathbf{r}-\mathbf{r}'|$, the distance from the field point $\mathbf{r}$ to the source point $\mathbf{r}'$ and $\nu = e$ or $d$. The magnetic surface charge density $\rho_s^m$ may be related to the magnetic surface current density by the continuity equation

$$\nabla \cdot \mathcal{M} = -\frac{\partial \rho_s^m}{\partial t}. \quad (10)$$

It may be noted that in general there is an electric scalar potential, $\nabla\Phi_\nu^e$, in equation (5). However, for TM incidence, the electric current density only has a $z$ component,

and we are assuming that all derivatives with respect to $z$ are zero; therefore $\nabla\Phi_\nu^e = 0$.

## 3. NUMERICAL SOLUTION PROCEDURE

In this section the numerical implementation of the EFIE, HFIE, and CFIE formulations using the method of moments is described to obtain a set of coupled marching-on-in-time equations.

### 3.1. Grid scheme and definition of basis functions

The grid scheme that is used is similar to that shown in Figure 2, and the actual cylinder is closed for penetrable objects. The body may be divided into rectangular patches. The $m$th zone has a width of $\Delta\xi_m$ and that whole column ($-\infty < z < \infty$) is divided into zones with $\Delta z = \Delta\xi_m$. Therefore the patch heights from one column to another are generally different. For simplicity, we will restrict ourselves to observing the current at $z = 0$ due to the invariance with respect to $z$.

We define a set of basis functions for expansion purposes as follows

$$f_m(\rho) = \begin{cases} 1 & \rho \in \rho_{m-\frac{1}{2}} \text{ to } \rho_{m+\frac{1}{2}} \\ 0 & \text{otherwise.} \end{cases} \tag{11}$$

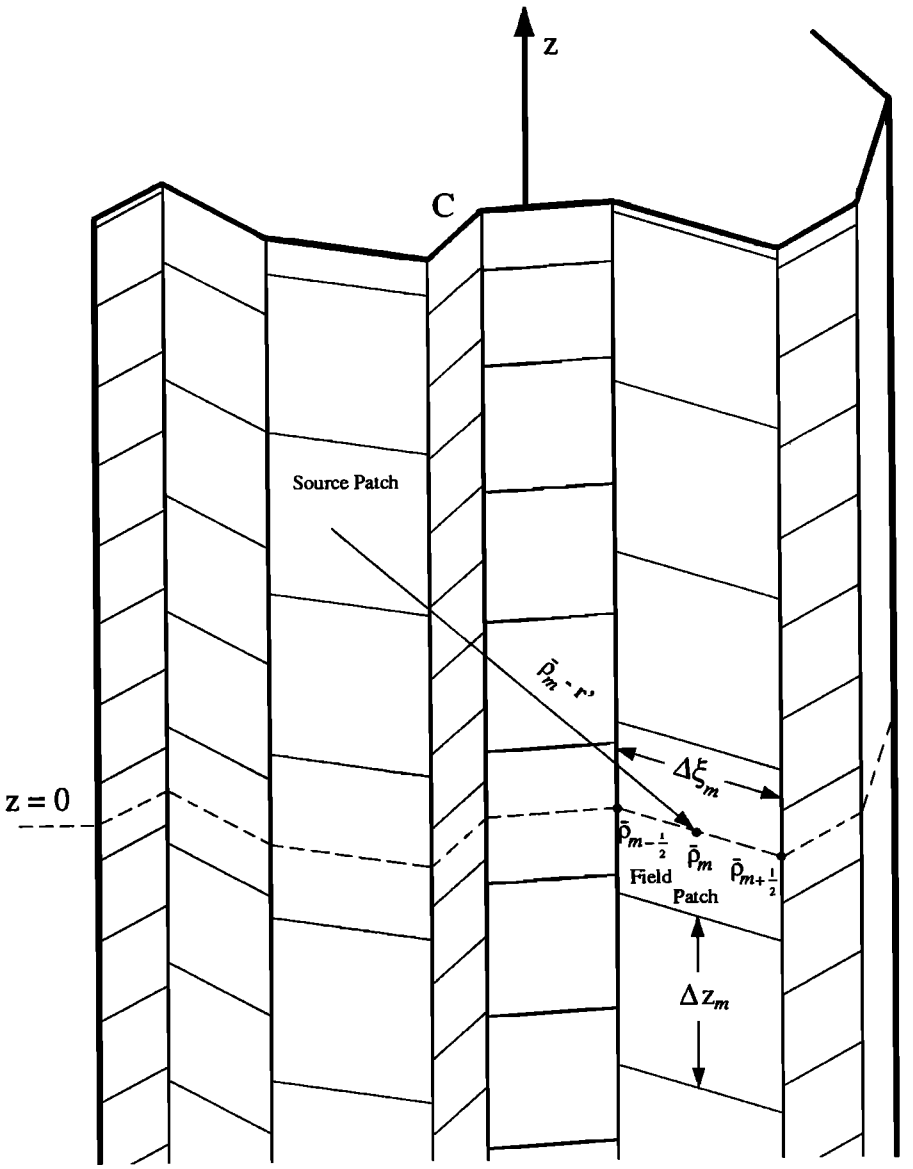


Fig. 2. The grid scheme used for dividing up the cylinder.

The $m,\ell$th patch is located between $\rho_{m-1/2}$ and $\rho_{m+1/2}$ along the contour and $z_\ell - \Delta z_m/2$ and $z_\ell + \Delta z_m/2$ along the $z$ axis, where $z_\ell = \ell \Delta z_m$. The patch centers are located at $(\rho_m, \ell\Delta z_m)$. These expansion functions are just the standard pulse functions on a rectangular patch. The testing functions will also be pulse functions, but since we are restricting ourselves to the $z = 0$ plane, they are defined along the contour to be

$$g_m(\rho) = \begin{cases} 1\hat{\mathbf{a}}_z & \rho \in \rho_{m-\frac{1}{2}} \text{ to } \rho_{m+\frac{1}{2}} \\ 0 & \text{otherwise.} \end{cases} \tag{12}$$

The inner product will be defined as

$$\langle a, b \rangle = \int_S a \cdot b \, ds'. \tag{13}$$

### 3.2. EFIE formulation

The EFIE formulation is obtained by using equations (1) and (3). Rewriting the scattered electric field in terms of the potential functions, taking an extra derivative with respect to time, and applying the testing procedure, gives

$$\left\langle g_m, \frac{\partial^2 \mathcal{A}_\nu}{\partial t^2} + \frac{1}{\varepsilon_\nu} \nabla \times \frac{\partial \mathcal{F}_\nu}{\partial t} \right\rangle = \begin{cases} \left\langle g_m, \frac{\partial \mathcal{E}^{\text{inc}}}{\partial t} \right\rangle \\ 0 \end{cases} \tag{14}$$

for $\nu = e$ or $d$. Even though it is not needed in this formulation, the extra derivative is introduced here so that when the fields are combined for the CFIE formulation, it may be of the same form as the magnetic field equation. Approximating the time derivatives of the potential functions by finite differences, we get

$$\langle g_m, L_\nu^{\text{E}}[\mathcal{J}, \mathcal{M}] \rangle = \begin{cases} \left\langle g_m, \frac{\partial \mathcal{E}^{\text{inc}}(t_n)}{\partial t} \right\rangle \\ 0 \end{cases}, \tag{15}$$

where

$$\begin{aligned} L_\nu^{\text{E}}[\mathcal{J}, \mathcal{M}] &= \frac{\mathcal{A}_\nu(\rho, t_{n+1}) - 2\mathcal{A}_\nu(\rho, t_n) + \mathcal{A}_\nu(\rho, t_{n-1})}{\Delta t^2} \\ &\quad + \frac{1}{\varepsilon_\nu} \nabla \times \left[ \frac{\mathcal{F}_\nu(\rho, t_{n+1}) - \mathcal{F}_\nu(\rho, t_n)}{\Delta t} \right] \end{aligned} \tag{16}$$

Note that the derivative $\partial \mathcal{F}_\nu / \partial t$ is approximated by using a forward difference scheme. This approximation is required in order to obtain a pair of linearly independent equations for $\mathcal{J}$ and $\mathcal{M}$. The incident field is assumed to be known so that its derivative may be evaluated analytically. Let

$$\mathcal{J}(\rho, t) = \hat{\mathbf{a}}_z \sum_{k=1}^{N} \mathcal{I}_k(t) f_k(\rho) \tag{17}$$

$$\mathcal{M}(\rho, t) = \hat{\mathbf{a}}_\xi \sum_{k=1}^{N} \mathcal{M}_k(t) f_k(\rho), \tag{18}$$

where $N$ is the number of linear segments along the contour $C$. Let us now look at the evaluation of $\mathcal{A}_\nu(\rho, t_n)$ and $\mathcal{F}_\nu(\rho, t_n)$, at a time $t_n$ and an observation point $\rho$ located in the $m$th patch. Combining equations (17) and (7) gives

$$\begin{aligned} \mathcal{A}_\nu(\rho, t_n) &= \frac{\mu_\nu}{4\pi} \int_C \int_{z'=-\infty}^{\infty} \frac{\hat{\mathbf{a}}_z \sum_{k=1}^{N} \mathcal{I}_k(t_n - \frac{R}{c_\nu}) f_k(\rho')}{R} dz' \, dC' \\ &= \frac{\mu_\nu}{4\pi} \sum_{k=1}^{N} \sum_{\ell=-\infty}^{\infty} \mathcal{I}_k(t_n - \frac{R_{mk\ell}}{c_\nu}) \kappa_{k,\ell} \hat{\mathbf{a}}_z, \end{aligned} \tag{19}$$

where

$$\begin{aligned} \kappa_{k,\ell} &= \int\int_{k,\ell \text{ patch}} \frac{ds'}{R}, \\ R &= \sqrt{|\rho - \rho'|^2 + z'^2}, \\ R_{mk\ell} &= \sqrt{|\rho_m - \rho_k|^2 + z_\ell'^2}. \end{aligned}$$

For nonself terms, that is, where $r$ and $r'$ do not belong to the same patch, the $1/R$ integral may be approximated by the patch area multiplied by the distance between the patch centers. For self terms, the integration is carried out analytically [*Damaskos et al.*, 1985]. The infinite summation on $\ell$ in equation (19) can actually be truncated to $-\ell_{\max} \le \ell \le \ell_{\max}$. Because of the retarded nature of the currents, we only need to extend the $\ell$ summation to a point where $t_n - R_{mk\ell}/c_\nu$ becomes negative. When $t_n - R_{mk\ell}/c_\nu < 0$, it implies that the solution has not yet progressed out far enough in time for those currents to have an effect at the observation point (assuming a causal system).

If $\Delta t$ is chosen appropriately, then there is only one current in equation (19) which is unknown, namely, when $k = m$ and $\ell = 0$ which implies $R_{mk\ell} = 0$. All the other currents are assumed known because they occur at some earlier time step. We may rewrite equation (19) as

$$\begin{aligned} \mathcal{A}_\nu(\rho, t_n) &= \frac{\mu_\nu \kappa_{m,0}}{4\pi} \mathcal{I}_m(t_n) \hat{\mathbf{a}}_z \\ &\quad + \frac{\mu_\nu}{4\pi} \sum_{\substack{k=1 \\ k \neq m}}^{N} \sum_{\substack{\ell=-\infty \\ \text{and } \ell \neq 0}}^{\infty} \mathcal{I}_k(t_n - \frac{R_{mk\ell}}{c_\nu}) \kappa_{k,\ell} \hat{\mathbf{a}}_z \\ &= \frac{\mu_\nu \kappa_m}{4\pi} \mathcal{I}_m(t_n) \hat{\mathbf{a}}_z + \not{\mathcal{A}}_\nu(\rho, t_n) \end{aligned} \tag{20}$$

where the $\ell = 0$ subscripts have been omitted and $\not{\mathcal{A}}_\nu(\rho, t_n)$ represents $\mathcal{A}_\nu(\rho, t_n)$ with the self term (i.e., $m = k$ and $\ell = 0$) deleted.

Next, let's consider the evaluation of the curl of the electric vector potential, $\frac{1}{\varepsilon_\nu} \nabla \times \mathcal{F}_\nu$. Using equation (8), taking the curl operator inside the integral, which is allowed as long as $R \neq 0$, and using the vector identity $\nabla \times (wA) = w \nabla \times A - A \times \nabla w$ gives

$$\frac{1}{\varepsilon_\nu}\nabla\times\not{\mathcal{F}}_\nu(\rho,t_n) = \frac{1}{4\pi}\iint_S \frac{\nabla\times\mathcal{M}(\rho',t_n-\frac{R}{c_\nu})}{R} - \mathcal{M}(\rho',t_n-\frac{R}{c_\nu})\times\nabla\frac{1}{R}\,ds'. \quad (21)$$

Note that

$$\nabla\frac{1}{R} = -\frac{\rho-\boldsymbol{r}'}{R^3} = -\frac{\hat{\mathbf{R}}}{R^2} \quad (22)$$

where $\hat{\mathbf{R}}$ is a unit vector in the direction of $\rho-\boldsymbol{r}'$. Letting $t_r = t_n - \frac{R}{c_\nu}$, we have

$$\nabla\times\mathcal{M}(\rho',t_n-\frac{R}{c_\nu}) = \nabla\times\mathcal{M}(\rho',t_r)\hat{\mathbf{a}}'_\xi = [\mathcal{M}(\rho',t_r)\nabla\times\hat{\mathbf{a}}'_\xi - \hat{\mathbf{a}}'_\xi\times\nabla\mathcal{M}(\rho',t_r)].$$

The $\nabla$ operator is operating on unprimed coordinates, so $\nabla\times\hat{\mathbf{a}}'_\xi = 0$. Using the vector identity $\nabla f(c(t_r)) = \partial f/\partial c(t_r)\cdot\nabla t_r$, we get

$$\nabla\times\mathcal{M}(\rho',t_n-\frac{R}{c_\nu}) = -\hat{\mathbf{a}}'_\xi\times\frac{\partial\mathcal{M}}{\partial t_r}\cdot\nabla t_r$$

$$\nabla t_r = \nabla(t_n-\frac{R}{c_\nu}) = \nabla t_n - \nabla\frac{R}{c_\nu} = -\frac{1}{c_\nu}\nabla R = -\frac{1}{c_\nu}\hat{\mathbf{R}}.$$

Thus

$$\nabla\times\mathcal{M}(\rho',t_n-\frac{R}{c_\nu}) = \frac{1}{c_\nu}\left(\frac{\partial\mathcal{M}}{\partial t_r}\hat{\mathbf{a}}'_\xi\times\hat{\mathbf{R}}\right). \quad (23)$$

Combining equations (21)–(23) then gives

$$\frac{1}{\varepsilon_\nu}\nabla\times\not{\mathcal{F}}_\nu(\rho,t_n) = \frac{1}{4\pi}\iint_S \frac{\mathcal{M}(\rho',t_n-\frac{R}{c_\nu})}{R^2}\hat{\mathbf{a}}'_\xi\times\hat{\mathbf{R}} + \frac{1}{Rc_\nu}\frac{\partial\mathcal{M}(\rho',t_r)}{\partial t_r}\hat{\mathbf{a}}'_\xi\times\hat{\mathbf{R}}\,ds'. \quad (24)$$

Now combining equations (18) and (24) results in

$$\frac{1}{\varepsilon_\nu}\nabla\times\not{\mathcal{F}}_\nu(\rho,t_n) = \frac{1}{4\pi}\sum_{\substack{k=1\\ k\neq m \text{ and } \ell\neq 0}}^{N}\sum_{\ell=-\infty}^{\infty}\mathcal{M}_k(t_n-\frac{R_{mk\ell}}{c_\nu})\iint_{k,\ell\ \text{patch}}\frac{\hat{\mathbf{a}}'_\xi\times\hat{\mathbf{R}}}{R^2}\,ds' + \frac{1}{4\pi c_\nu}\sum_{\substack{k=1\\ k\neq m \text{ and } \ell\neq 0}}^{N}\sum_{\ell=-\infty}^{\infty}\frac{\partial\mathcal{M}_k(t_r)}{\partial t_r}\iint_{k,\ell\ \text{patch}}\frac{\hat{\mathbf{a}}'_\xi\times\hat{\mathbf{R}}}{R}\,ds'. \quad (25)$$

Even though there are three components from the cross product, only the $\hat{\mathbf{a}}_z$ component "survives" because of the symmetry. As before, the nonself term integrals may be approximated by the patch area times the integrand evaluated at the patch centers. The $\partial\mathcal{M}_k/\partial t_r$ term is approximated by a first-order backward difference

$$\frac{\partial\mathcal{M}_k(t_r)}{\partial t_r} \approx \frac{\mathcal{M}_k(t_n-\frac{R_{mk\ell}}{c_\nu}) - \mathcal{M}_k(t_{n-1}-\frac{R_{mk\ell}}{c_\nu})}{\Delta t}.$$

Finally, the curl of the vector potential may be written as

$$\frac{1}{\varepsilon_\nu}\nabla\times\mathcal{F}_\nu(\rho,t_n) = \pm\frac{\mathcal{M}_m(t_n)}{2}\hat{\mathbf{a}}_z + \frac{1}{\varepsilon_\nu}\nabla\times\not{\mathcal{F}}_\nu(\rho,t_n). \quad (26)$$

Note that the $\pm\mathcal{M}_m/2$ is obtained by extracting the Cauchy principal value from the curl term. The plus sign is for $\nu = e$, and the minus sign is for $\nu = d$.

Finally, if we replace $n \Rightarrow n-1$, combine equations (15), (20), and (26), take all known quantities $(n-1, n-2, \ldots)$ to the right side, and use a 1-point integration for the testing procedure, we get the following pair of equations:

$$\frac{\mu_e\kappa_m\Delta\xi_m}{4\pi\Delta t^2}\mathcal{I}_m(t_n) + \frac{\Delta\xi_m}{2\Delta t}\mathcal{M}_m(t_n) = \langle g_m, \boldsymbol{Y}_e^{\mathrm{E}}\rangle, \quad (27)$$

$$\frac{\mu_d\kappa_m\Delta\xi_m}{4\pi\Delta t^2}\mathcal{I}_m(t_n) - \frac{\Delta\xi_m}{2\Delta t}\mathcal{M}_m(t_n) = \langle g_m, \boldsymbol{Y}_d^{\mathrm{E}}\rangle, \quad (28)$$

where

$$\boldsymbol{Y}_e^{\mathrm{E}} = \frac{\partial\mathcal{E}^{\mathrm{inc}}(t_{n-1})}{\partial t} - \not{L}_e^{\mathrm{E}}[\mathcal{J},\mathcal{M}], \quad (29)$$

$$\boldsymbol{Y}_d^{\mathrm{E}} = -\not{L}_d^{\mathrm{E}}[\mathcal{J},\mathcal{M}], \quad (30)$$

$$\not{L}_\nu^{\mathrm{E}}[\mathcal{J},\mathcal{M}] = \frac{\not{\mathcal{A}}_\nu(\rho_m,t_n) - 2\mathcal{A}_\nu(\rho_m,t_{n-1}) + \mathcal{A}_\nu(\rho_m,t_{n-2})}{\Delta t^2} + \frac{1}{\varepsilon_\nu}\nabla\times\left[\frac{\not{\mathcal{F}}_\nu(\rho_m,t_n) - \mathcal{F}_\nu(\rho_m,t_{n-1})}{\Delta t}\right]. \quad (31)$$

By examining equations (27) and (28) it is evident that the left-hand side only involves terms at $t = t_n$, while the right-hand side contains the terms retarded in time. Therefore, the currents may be obtained by the marching-on-in-time procedure. Once the currents at $t_n$ are found for all $1 \le m \le N$, the time step is incremented, and the currents at $t_{n+1}$ can then be found in the same manner since all of the previous currents are known. Thus, the numerical procedure starts at $n = 2$, assuming everything zero at $n = 0$ and $n = 1$, and then marches on in time for $n = 3, 4, 5, \ldots$. An important factor to note in deriving equations (27) and (28) is that the time step $\Delta t$ should be less than $R_{\min}/\max\{c_e, c_d\}$, where $R_{\min}$ is the minimum distance between patch centers. This allows the currents to be solved for explicitly without the need for matrix inversion. However, Courant's stability condition dictates that in order to generate a stable numerical result $\Delta t \le R_{\min}/(\max\{c_e, c_d\}\sqrt{2})$ [*Rynne and Smith*, 1990], and in the present work we chose $\Delta t = 0.5R_{\min}/\max\{c_e, c_d\}$.

### 3.3. HFIE Formulation

The HFIE formulation is obtained by using equations (2) and (4). Rewriting the scattered magnetic field in terms of the potentials, taking an extra derivative with respect to time, and applying the testing procedure, gives

$$\left\langle g_m, \hat{\mathbf{a}}_n \times \left[ \frac{\partial^2 \mathcal{F}_\nu}{\partial t^2} + \nabla \frac{\partial \Phi_\nu^m}{\partial t} - \frac{1}{\mu_\nu} \nabla \times \frac{\partial \mathcal{A}_\nu}{\partial t} \right] \right\rangle = \begin{cases} \left\langle g_m, \hat{\mathbf{a}}_n \times \frac{\partial \mathcal{H}^{\text{inc}}}{\partial t} \right\rangle \\ 0 \end{cases} . \quad (32)$$

The extra derivative is taken so that the continuity equation (10) may be used. Following similar steps as in the EFIE, we obtain

$$\langle g_m, \hat{\mathbf{a}}_n \times L_\nu^{\text{H}}[\mathcal{J}, \mathcal{M}] \rangle = \begin{cases} \left\langle g_m, \hat{\mathbf{a}}_n \times \frac{\partial \mathcal{H}^{\text{inc}_{(t_n)}}}{\partial t} \right\rangle \\ 0 \end{cases} , \quad (33)$$

where

$$L_\nu^{\text{H}}[\mathcal{J}, \mathcal{M}] = \frac{\mathcal{F}_\nu(\rho, t_{n+1}) - 2\mathcal{F}_\nu(\rho, t_n) + \mathcal{F}_\nu(\rho, t_{n-1})}{\Delta t^2} + \nabla \Psi_\nu^m(\rho, t_n) - \frac{1}{\mu_\nu} \nabla \times \left[ \frac{\mathcal{A}_\nu(\rho, t_{n+1}) - \mathcal{A}_\nu(\rho, t_n)}{\Delta t} \right] \quad (34)$$

and

$$\Psi_\nu^m = \frac{\partial \Phi_\nu^m}{\partial t}. \quad (35)$$

Next, the current expansions of equations (17) and (18) will be used to expand the operator $L_\nu^{\text{H}}[\mathcal{J}, \mathcal{M}]$. The evaluation of $\mathcal{F}_\nu$ is very similar to the determination of $\mathcal{A}_\nu$ in the EFIE. The only difference is that the currents are in the circumferential direction. Therefore

$$\begin{aligned} \mathcal{F}_\nu(\rho, t_n) &= \frac{\varepsilon_\nu}{4\pi} \sum_{k=1}^{N} \sum_{\ell=-\infty}^{\infty} \mathcal{M}_k(t_n - \frac{R_{mk\ell}}{c_\nu}) \kappa_{k,\ell} \hat{\mathbf{a}}_\xi \\ &= \frac{\varepsilon_\nu \kappa_m}{4\pi} \mathcal{M}_m(t_n) \hat{\mathbf{a}}_\xi + \not{\mathcal{F}}_\nu(\rho, t_n). \end{aligned} \quad (36)$$

Likewise,

$$\begin{aligned} \frac{1}{\mu_\nu} \nabla \times \not{\mathcal{A}}_\nu(\rho, t_n) = & \frac{1}{4\pi} \sum_{\substack{k=1 \\ k \neq m \text{ and } \ell \neq 0}}^{N} \sum_{\ell=-\infty}^{\infty} \mathcal{I}_k(t_n - \frac{R_{mk\ell}}{c_\nu}) \iint_{k,\ell \text{ patch}} \frac{\hat{\mathbf{a}}_z \times \hat{\mathbf{R}}}{R^2} ds' \\ & + \frac{1}{4\pi c_\nu} \sum_{\substack{k=1 \\ k \neq m \text{ and } \ell \neq 0}}^{N} \sum_{\ell=-\infty}^{\infty} \frac{\partial \mathcal{I}_k(t_r)}{\partial t_r} \iint_{k,\ell \text{ patch}} \frac{\hat{\mathbf{a}}_z \times \hat{\mathbf{R}}}{R} ds' \end{aligned}$$

$$\frac{1}{\mu_\nu} \nabla \times \mathcal{A}_\nu = \mp \frac{\mathcal{I}_m(t_n)}{2} \hat{\mathbf{a}}_\xi + \frac{1}{\mu_\nu} \nabla \times \not{\mathcal{A}}_\nu(\rho, t_n). \quad (37)$$

We now turn our attention to the evaluation of $\nabla \Psi_\nu^m(\rho, t_n)$. By changing the order of the scalar product and using the fact that the line integral of the gradient of a potential function is the function evaluated at its endpoints, we can rewrite the gradient term as

$$\begin{aligned} \langle g_m, \hat{\mathbf{a}}_n \times \nabla \Psi_\nu^m(\rho, t_n) \rangle &= \int_S \nabla \Psi_\nu^m(\rho, t_n) \cdot g_m \times \hat{\mathbf{a}}_n \, ds' \\ &= \Psi_\nu^m(\rho_{m+\frac{1}{2}}, t_n) - \Psi_\nu^m(\rho_{m-\frac{1}{2}}, t_n). \end{aligned} \quad (38)$$

Combining equations (9), (10), and (35) gives

$$\Psi_\nu^m(\rho_{m+\frac{1}{2}}, t_n) = \frac{1}{4\pi\mu_\nu} \int_C \int_{z'=-\infty}^{\infty} \frac{-\partial \mathcal{M}(\rho', t_n - \frac{R}{c_\nu})/\partial \xi}{R} dz' dC', \quad (39)$$

where $R = (|\rho_{m+\frac{1}{2}} - \mathbf{r}'|^2 + z'^2)^{1/2}$. Note that in equation (39) the derivative is with respect to the first argument only. Using equation (18) for the expansion of $\mathcal{M}$ in (39) results in

$$\Psi_\nu^m(\rho_{m+\frac{1}{2}}, t_n) = \frac{1}{4\pi\mu_\nu} \sum_{k=1}^{N} \sum_{\ell=-\infty}^{\infty} -\mathcal{M}_k(t_n - \frac{R_{mk\ell}}{c_\nu}) \times \iint_{k,\ell \text{ patch}} \frac{\partial f_k / \partial \xi}{R} ds'. \quad (40)$$

Since pulse basis functions are being used, $\partial f_k / \partial \xi$ results in two delta functions; one at $\rho_{k+1/2}$ and one at $\rho_{k-1/2}$. We can spread the "effect" of these delta functions across the contour from $\rho_{k-1}$ to $\rho_{k+1}$. This basically amounts to approximating the derivative by a finite difference. We can now express equation (40) as

$$\Psi_\nu^m(\rho_{m+\frac{1}{2}}, t_n) = \sum_{k=1}^{N} \sum_{\ell=-\infty}^{\infty} \Psi_\nu^{m+}(\rho_{m+\frac{1}{2}}, t_n) - \Psi_\nu^{m-}(\rho_{m+\frac{1}{2}}, t_n), \quad (41)$$

where

$$\Psi_\nu^{m+}(\rho_{m+\frac{1}{2}}, t_n) = \frac{-1}{4\pi\mu_\nu} \frac{\mathcal{M}_k(t_n - \frac{R_{mk\ell}^+}{c_\nu})}{\Delta \xi_k^+} \times \int_{\rho_{k-1}}^{\rho_k} \int_{z_1}^{z_2} \frac{d\ell' \, dz'}{\sqrt{|\rho_{m+\frac{1}{2}} - \rho'|^2 + z'^2}}, \quad (42)$$

$$\Psi_\nu^{m-}(\rho_{m+\frac{1}{2}}, t_n) = \frac{-1}{4\pi\mu_\nu} \frac{\mathcal{M}_k(t_n - \frac{R_{mk\ell}^-}{c_\nu})}{\Delta \xi_k^-} \times \int_{\rho_k}^{\rho_{k+1}} \int_{z_1}^{z_2} \frac{d\ell' \, dz'}{\sqrt{|\rho_{m+\frac{1}{2}} - \rho'|^2 + z'^2}}, \quad (43)$$

with

$$\begin{aligned} R_{mk\ell}^+ &= \sqrt{|\rho_{m+\frac{1}{2}} - \rho_{k-\frac{1}{2}}|^2 + z'^2}, \\ R_{mk\ell}^- &= \sqrt{|\rho_{m+\frac{1}{2}} - \rho_{k+\frac{1}{2}}|^2 + z'^2}, \\ \Delta \xi_k^+ &= |\rho_k - \rho_{k-1}|, \\ \Delta \xi_k^- &= |\rho_{k+1} - \rho_k|, \\ z_1 &= z_\ell - \frac{\Delta z_k}{2}, \\ z_2 &= z_\ell + \frac{\Delta z_k}{2}. \end{aligned}$$

While calculating $\Psi_\nu^m(\rho_{m+1/2}, t_n)$, some computational time may be saved by observing that the integral for $\Psi_\nu^{m-}$

is the same as that for $\Psi_\nu^{m+}$. The currents, however, are not the same so an interpolation still needs to be done. The calculation of $\Psi_\nu^m(\rho_{m-1/2}, t_n)$ proceeds exactly the same as $\Psi_\nu^m(\rho_{m+1/2}, t_n)$ except that $\rho_{m+1/2}$ is replaced with $\rho_{m-1/2}$. Computational time can also be decreased when we move to the next field point by observing the fact that $\Psi_\nu^m(\rho_{m+1/2}, t_n) = \Psi_\nu^m(\rho_{m'-1/2}, t_n)$ when $m' = m+1$.

By combining equations (34)–(37) and equations (41)–(43), replacing $n \Rightarrow n-1$, taking all the known quantities (those involving currents prior to and including $t_{n-1}$) to the right, and using a 1-point integration for the testing procedure, gives

$$\frac{\Delta\xi_m}{2\Delta t}\mathcal{I}_m(t_n) + \frac{\varepsilon_e\kappa_m\Delta\xi_m}{4\pi\Delta t^2}\mathcal{M}_m(t_n) = \langle g_m, \hat{\mathbf{a}}_n \times \boldsymbol{Y}_e^{\mathrm{H}}\rangle, \quad (44)$$

$$-\frac{\Delta\xi_m}{2\Delta t}\mathcal{I}_m(t_n) + \frac{\varepsilon_d\kappa_m\Delta\xi_m}{4\pi\Delta t^2}\mathcal{M}_m(t_n) = \langle g_m, \hat{\mathbf{a}}_n \times \boldsymbol{Y}_d^{\mathrm{H}}\rangle, \quad (45)$$

where

$$\boldsymbol{Y}_e^{\mathrm{H}} = \frac{\partial\mathcal{H}^{\mathrm{inc}}(t_{n-1})}{\partial t} - \not{L}_e^{\mathrm{H}}[\mathcal{J}, \mathcal{M}], \quad (46)$$

$$\boldsymbol{Y}_d^{\mathrm{H}} = -\not{L}_d^{\mathrm{H}}[\mathcal{J}, \mathcal{M}], \quad (47)$$

$$\not{L}_\nu^{\mathrm{H}}[\mathcal{J}, \mathcal{M}] = \nabla\Psi_\nu^m(\rho_m, t_{n-1}) + \frac{\not{\mathcal{F}}_\nu(\rho_m, t_n) - 2\mathcal{F}_\nu(\rho_m, t_{n-1}) + \mathcal{F}_\nu(\rho_m, t_{n-2})}{\Delta t^2} - \frac{1}{\mu_\nu}\nabla\times\left[\frac{\not{\mathcal{A}}_\nu(\rho_m, t_n) - \mathcal{A}_\nu(\rho_m, t_{n-1})}{\Delta t}\right]. \quad (48)$$

Equations (44) and (45) can then be used with the marching-on-in-time technique to solve for the currents $\mathcal{I}_m(t_n)$ and $\mathcal{M}_m(t_n)$.

### 3.4. CFIE formulation

The equations for the CFIE will follow quickly since most of the work has been done in the EFIE and HFIE formulations. The CFIE is obtained by forming two new equations by taking $\alpha(1) + \hat{\mathbf{a}}_n \times \eta_e(1-\alpha)(2)$ and $\alpha(3) + \hat{\mathbf{a}}_n \times \eta_e(1-\alpha)(4)$, where $0 \le \alpha \le 1$. Taking $\alpha(14) + \eta_e(1-\alpha)(32)$ and using the field operators from equations (16) and (34), we obtain

$$\langle g_m, \alpha\boldsymbol{L}_\nu^{\mathrm{E}}[\mathcal{J}, \mathcal{M}] + \hat{\mathbf{a}}_n \times \eta_e(1-\alpha)\boldsymbol{L}_\nu^{\mathrm{H}}[\mathcal{J}, \mathcal{M}]\rangle = \begin{cases} \left\langle g_m, \alpha\frac{\partial\mathcal{E}^{\mathrm{inc}}}{\partial t} + \hat{\mathbf{a}}_n \times \eta_e(1-\alpha)\frac{\partial\mathcal{H}^{\mathrm{inc}}}{\partial t}\right\rangle \\ 0 \end{cases}. \quad (49)$$

Replacing $n \Rightarrow n-1$ and taking all known quantities to the right gives

$$a_{11}\mathcal{I}_m(t_n) + a_{12}\mathcal{M}_m(t_n) = \langle g_m, \alpha\boldsymbol{Y}_e^{\mathrm{E}} + \hat{\mathbf{a}}_n \times \eta_e(1-\alpha)\boldsymbol{Y}_e^{\mathrm{H}}\rangle, \quad (50)$$

$$a_{21}\mathcal{I}_m(t_n) + a_{22}\mathcal{M}_m(t_n) = \langle g_m, \alpha\boldsymbol{Y}_d^{\mathrm{E}} + \hat{\mathbf{a}}_n \times \eta_e(1-\alpha)\boldsymbol{Y}_d^{\mathrm{H}}\rangle, \quad (51)$$

where

$$a_{11} = \alpha\frac{\mu_e\kappa_m\Delta\xi_m}{4\pi\Delta t^2} + \eta_e(1-\alpha)\frac{\Delta\xi_m}{2\Delta t}, \quad (52)$$

$$a_{12} = \alpha\frac{\Delta\xi_m}{2\Delta t} + \eta_e(1-\alpha)\frac{\varepsilon_e\kappa_m\Delta\xi_m}{4\pi\Delta t^2}, \quad (53)$$

$$a_{21} = \alpha\frac{\mu_d\kappa_m\Delta\xi_m}{4\pi\Delta t^2} - \eta_e(1-\alpha)\frac{\Delta\xi_m}{2\Delta t}, \quad (54)$$

$$a_{22} = \alpha\frac{-\Delta\xi_m}{2\Delta t} + \eta_e(1-\alpha)\frac{\varepsilon_d\kappa_m\Delta\xi_m}{4\pi\Delta t^2}, \quad (55)$$

where $\not{L}_\nu^{\mathrm{E}}[\mathcal{J}, \mathcal{M}]$ and $\not{L}_\nu^{\mathrm{H}}[\mathcal{J}, \mathcal{M}]$ are defined by equations (31), and (48), while $\boldsymbol{Y}_e^{\mathrm{E}}$, $\boldsymbol{Y}_d^{\mathrm{E}}$, $\boldsymbol{Y}_e^{\mathrm{H}}$, and $\boldsymbol{Y}_d^{\mathrm{H}}$ are given by equations (29), (30), (46), and (47), respectively.

### 3.5. Stabilization of the late-time oscillations

The numerical solution procedure, discussed so far, has the tendency to become unstable at late-times even after satisfying the Courant stability condition. This phenomenon is common to most of the time-marching methods, and a number of different causes were attributed such as insufficient sampling, possibility of internal resonances, and/or errors caused while evaluating various intermediate quantities. Furthermore, there are a number of different techniques that are proposed to overcome this problem [*Mieras*, 1984; *Tijhuis*, 1984; *Rynne*, 1986; *Rynne*, 1991]. In the present work, we propose an averaging scheme which is simple, accurate, and involves a negligible amount of extra computation.

First, the currents were found to sometimes grow quite quickly, even before the peak of the incident pulse had arrived. This was believed to be attributed to numerical problems with the relative difference in the magnitude of the electric and magnetic currents. The magnetic currents generally being approximately a factor of $\eta$ larger. Therefore, if we scale $\mathcal{M}$ by the constant $\eta_e$, (i.e., let $\mathcal{M} = \eta_e\mathcal{M}'$) and solve for $\mathcal{I}$ and $\mathcal{M}'$, the currents will be of the same order. When scaling was used, better results were obtained. However, late-time oscillations were still present which may be eliminated by the following averaging procedure. Let $\mathcal{I}_{m,j}$ and $\mathcal{M}_{m,j}$ be the current coefficients at the $m$th zone at a time instant $j\Delta t$. In the present stabilization scheme, we calculate $\mathcal{I}_{m,j+1}$ and $\mathcal{M}_{m,j+1}$ using equations (27) and (28) for the EFIE, (44) and (45) for the HFIE, or (50) and (51) for the CFIE, and simply approximate the averaged values of $\widetilde{\mathcal{I}}_{m,j}$ and $\widetilde{\mathcal{M}}_{m,j}$ by

$$\widetilde{\mathcal{I}}_{m,j} = \frac{1}{4}(\widetilde{\mathcal{I}}_{m,j-1} + 2\mathcal{I}_{m,j} + \mathcal{I}_{m,j+1}) \quad (56)$$

$$\widetilde{\mathcal{M}}_{m,j} = \frac{1}{4}(\widetilde{\mathcal{M}}_{m,j-1} + 2\mathcal{M}_{m,j} + \mathcal{M}_{m,j+1}). \quad (57)$$

Thus, in the present method, we need to add an extra step to the normal marching-on-in-time algorithm, and obviously, this step involves very little processing time. Moreover, it should be noted that this averaging scheme would

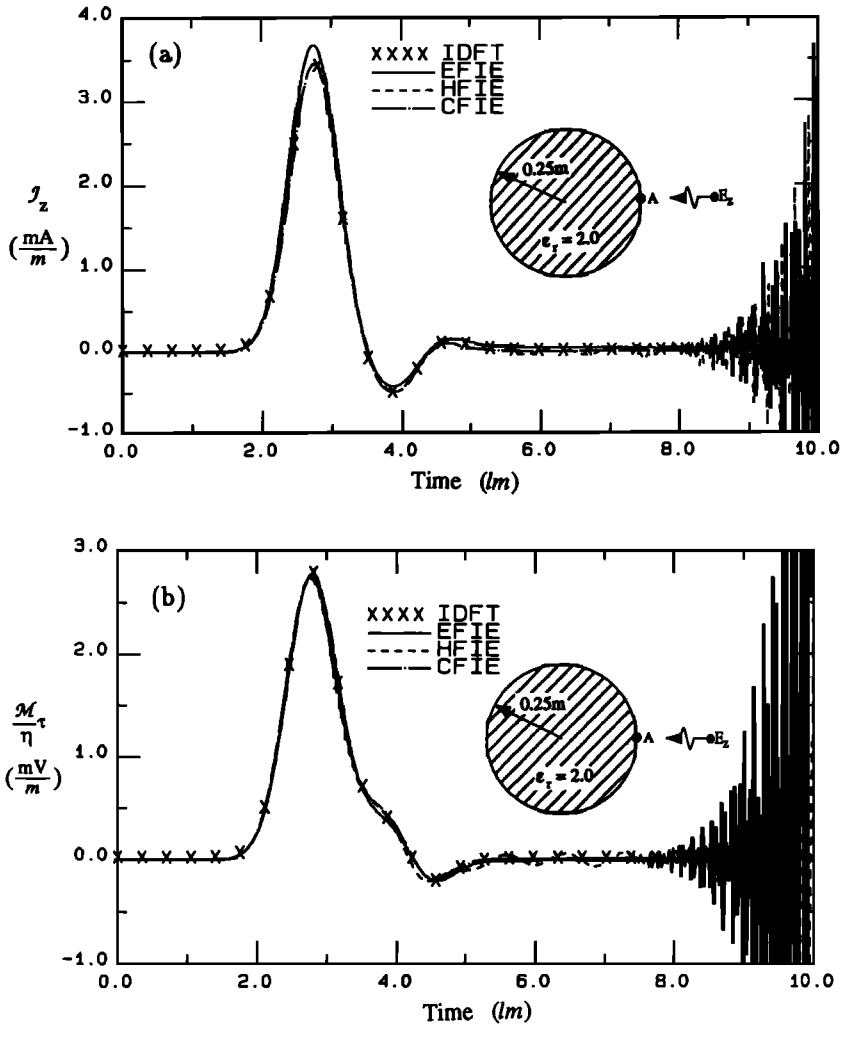


Fig. 3. Equivalent (a) electric and (b) magnetic currents at point A on a dielectric circular cylinder illuminated by a Gaussian plane-wave. The cylinder was divided into 28 segments along its perimeter, and no averaging was performed.

be the same as the one presented by *Rynne* [1991], if we recompute $\mathcal{I}_{m,j+1}$ and $\mathcal{M}_{m,j+1}$ after computing $\widetilde{\mathcal{I}}_{m,j}$ and $\widetilde{\mathcal{M}}_{m,j}$ using equations (56) and (57). However, we observed that the recomputation of $\mathcal{I}_{m,j+1}$ and $\mathcal{M}_{m,j+1}$ was not necessary and in some instances led to unstable results.

## 4. NUMERICAL RESULTS

In this section, we present numerical results for the equivalent currents on circular and square dielectric cylinders illuminated by a Gaussian plane-wave. The results are compared with data obtained in the frequency domain and transformed into the time domain by using inverse discrete Fourier transform techniques (IDFT). The method of moments was employed for calculating the frequency domain solutions.

The incident electric field is a Gaussian plane-wave of the form

$$\mathcal{E}^{\text{inc}}(\rho,t) = E_o \frac{4}{T\sqrt{\pi}} e^{-\gamma^2} \hat{\mathbf{a}}_z$$

with

$$\gamma = \frac{4}{T}(c_e t - c_e t_o - \boldsymbol{\rho}\cdot\hat{\mathbf{k}}),$$

where $c_e$ is the velocity of propagation in the external medium, $\hat{\mathbf{k}}$ is a unit vector in the direction of propagation of the incident wave, $T$ is the pulse width of the Gaussian impulse, and at $t = t_o$ the Gaussian pulse reaches its maximum value. The pulse width $T$ is defined such that for $c_e t - c_e t_o - \boldsymbol{\rho}\cdot\hat{\mathbf{k}} = \pm T/2$ the exponential has fallen to about 2% of its peak value. The results in this work were obtained with $E_o = 1.0$, $\hat{\mathbf{k}} = -\hat{\mathbf{a}}_x$, $T = 2.0$ lm (light-

meter), and $c_e t_o = 3.0$ lm. Note that 1 lm is the unit of time taken by the electromagnetic wave to propagate a distance of 1.0 m in free space. The external parameters were $\varepsilon_r = 1.0$ and $\mu_r = 1.0$, while the internal parameters were $\varepsilon_r = 2.0$ and $\mu_r = 1.0$. The CFIE results were obtained with $\alpha = 0.2$.

We first consider a circular cylinder with a radius of 0.25 m and centered about the origin. The contour was divided into 28 zones, and the time step was $c_e \Delta t = 0.02764$ lm. The frequency domain solution was obtained by calculating the currents for a range of frequencies and then using a discrete inverse Fourier transform. At a specific frequency, the incident field was weighted by an amount proportional to the magnitude of the frequency component of the incident pulse at that frequency. The range of frequencies for this problem was from 0 to 1.0 GHz with 256 sample points. Figure 3 shows the equivalent electric and magnetic currents at $\phi = 0°$ obtained by the various formulations discussed earlier. All three formulations agree very well with the frequency domain solution. The averaging algorithm was not employed here, and as can be seen, late-time instabilities have set in. The CFIE also suffers from a late-time instability. This suggests that the instabilities are not solely due to internal resonances. The same currents are shown in Figure 4 with the averaging process included. Again, the agreement is very good and the late-time instabilities have been removed.

Next, a square cylinder is considered. This geometry is 1.0 m on a side and is centered about the origin. The time domain solution used a total of 40 zones while the frequency domain solution used 80 zones. This allowed the currents to be obtained at the same locations due to

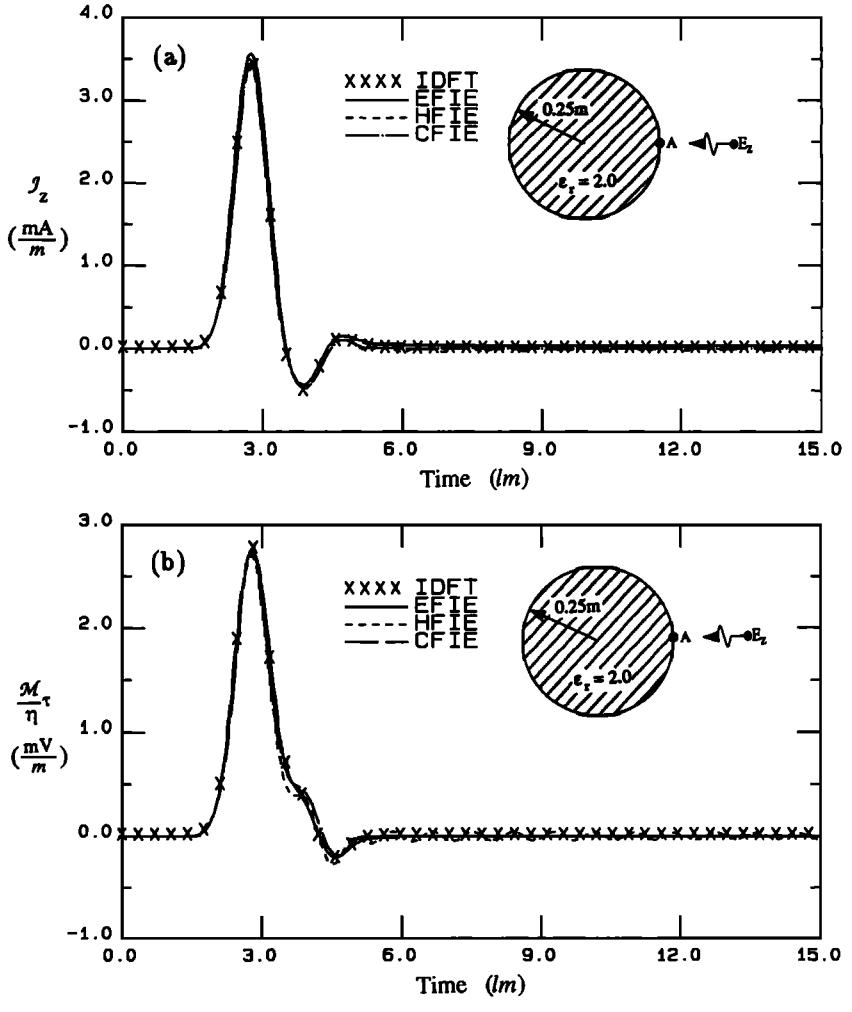


Fig. 4. Equivalent (a) electric and (b) magnetic currents at point A on a dielectric circular cylinder illuminated by a Gaussian plane-wave. The cylinder was divided into 28 segments along its perimeter and averaging was performed on the currents.

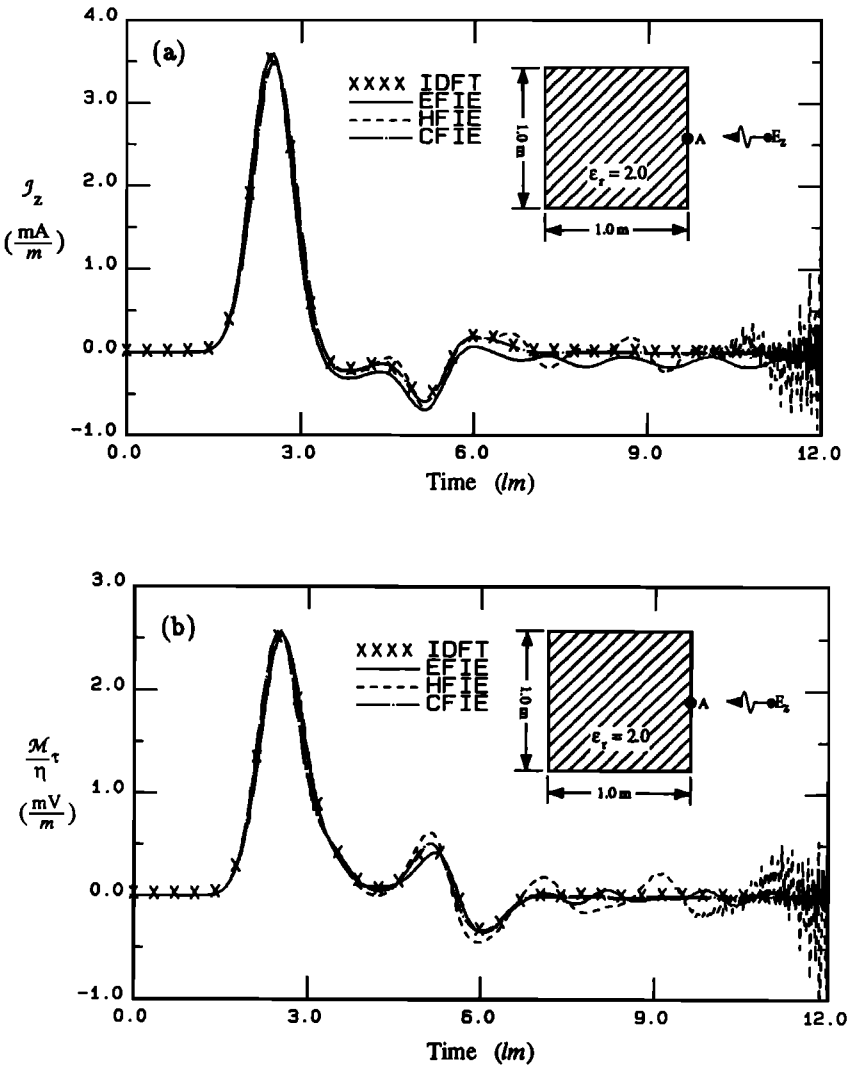


Fig. 5. Equivalent (a) electric and (b) magnetic currents at point A on a dielectric square cylinder illuminated by a Gaussian plane-wave. The cylinder was divided into 40 zones (80 zones for the IDFT), and no averaging was performed.

a slight difference in the way the two results were computed which results in a half zone shift in the discretized contours. The time step was $c_e \Delta t = 0.3536$ lm. The frequency domain solution considered frequencies between 0 and 1.0 GHz with 256 sample points. The unaveraged electric and scaled magnetic currents at the center of the lit side are shown in Figure 5. The time domain solutions compare very well with the frequency solution in the early time. After the main pulse passes the differences are larger for the EFIE and the HFIE. Again, late-time instabilities arise in the three formulations. Figure 6 shows the electric and magnetic currents when the averaging process is used. The currents agree very well during the main pulse, and the instabilities have been removed. The CFIE appears to agree better than the EFIE and HFIE.

## 5. SUMMARY AND CONCLUSIONS

In this work the marching-on-in-time technique has been used to solve the transient scattering problem of two-dimensional homogeneous dielectric cylinders of arbitrary shape. Using the surface equivalence principle, a set of coupled integral equations were derived. The objective was to

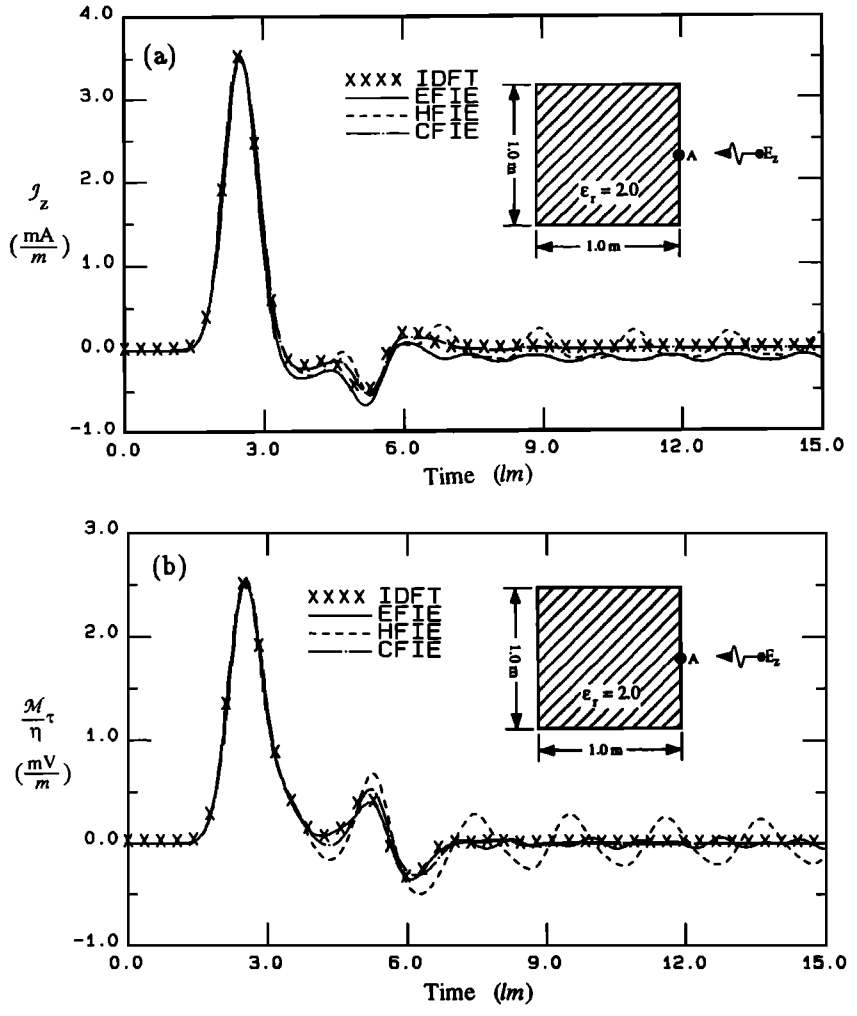


Fig. 6. Equivalent (a) electric and (b) magnetic currents at point A on a dielectric square cylinder illuminated by a Gaussian plane-wave. The cylinder was divided into 40 zones (80 zones for the IDFT), and averaging was performed on the currents.

develop alternate formulations to see if the late-time instabilities are due to the nonuniqueness of the solution of the integral equation. Three formulations, namely, the EFIE, HFIE, and CFIE were derived. The solution procedure was based on the method of moments, and the numerical results were in good agreement with those obtained by inverse discrete Fourier transform techniques. However, late-time instabilities were present in all three formulations suggesting that the oscillations are not entirely due to the internal resonances alone. A simple and efficient averaging scheme was also presented which removed the late-time instabilities. The stable results were also in good agreement with alternate methods.

Acknowledgments. This work was sponsored by the NASA Langley Research Center, Hampton Virginia.

## REFERENCES

Bennett, Jr., C. L., A technique for computing approximate electromagnetic impulse response of conducting bodies, Ph.D. dissertation, Purdue Univ., West Lafayette, Ind., 1968.

Bennett, Jr., C. L., and G. F. Ross, Time-domain electromagnetics and its applications, *Proc. IEEE*, 66, 299–318, 1978.

Damaskos, N. J., R. T. Brown, J. R. Jameson, and P. L. E. Uslenghi, Transient scattering by resistive cylinders, *IEEE Trans. Antennas Propag.*, AP-33, 21–25, 1985.

Kishk, A. A., and L. Shafai, Different formulations for numerical solution of single and multibodies of revolution with mixed boundary conditions, *IEEE Trans. Antennas Propag.*, AP-34, 666–673, 1986.

Mautz, J. R., and R. F. Harrington, H-Field, E-field, and combined-field solutions for conducting bodies of revolution, Arch. Elektron. Uebentraegungstech. (in German), 32(4), 157–164, 1978.

Mieras, H., Local influence technique in time domain scattering, Ph.D. dissertation, Northeastern Univ., Boston, Mass., 1984.

Miller, E. K., A. J. Poggio, and G. J. Burke, An integro-differential equation technique for the time-domain analysis of thin-wire structures, Part I, The numerical method, *J. Comp. Phys.*, 12(1–2), 1973.

Rao, S. M., and D. R. Wilton, Transient scattering by conducting surfaces of arbitrary shape, *IEEE Trans. Antennas Propag.*, AP-39, 56–61, 1991.

Rynne, B. P., Instabilities in time marching methods for scattering problems, *Electromagnetics*, 6, 129–144, 1986.

Rynne, B. P., Time domain scattering from arbitrary surfaces using the electric field integral equation, *J. Electromagn. Waves Appl.*, 5, 93–112, 1991.

Rynne, B. P., and P. D. Smith, Stability of time marching algorithms for the electric field integral equation, *J. Electromagn. Waves Appl.*, 4, 1181–1205, 1990.

Smith, P. D., Instabilities in time marching methods for scattering: cause and rectification, *Electromagnetics*, 10, 439–451, 1990.

Tijhuis, A. G., Towards a stable marching-on-in-time method for two dimensional transient electromagnetic scattering problems, *Radio Sci.*, 19, 1311–1317, 1984.

S. M. Rao, Department of Electrical Engineering, 200 Broun Hall, Auburn University, Auburn, AL 36849-5201.

D. A. Vechinski, Lockheed Advanced Development Company, P.O. Box 250, Sunland, CA 91041